

Graphdiyne as a Host Active Material for Perovskite Solar Cell Application

Jiangsheng Li,[†] Tonggang Jiu,^{*,†,§,⊥} Siqi Chen,[†] Le Liu,[†] Quantong Yao,[†] Fuzhen Bi,[†] Chengjie Zhao,[†] Zhen Wang,[†] Min Zhao,[†] Guodong Zhang,[†] Yurui Xue,[‡] Fushen Lu,^{||} and Yuliang Li^{*,†,§}

[†]Qingdao Institute of Bioenergy and Bioprocess Technology, Chinese Academy of Sciences, Qingdao 266101, PR China

[‡]Beijing National Laboratory for Molecular Sciences (BNLMS), Institute of Chemistry, Chinese Academy of Sciences, Beijing 100190, PR China

[§]University of Chinese Academy of Sciences, Beijing 100049, PR China

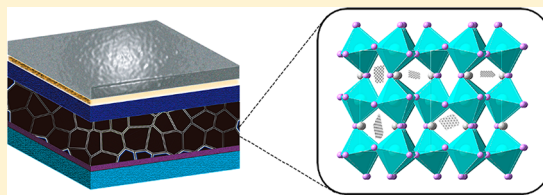
^{||}Department of Chemistry and Key Laboratory for Preparation and Application of Ordered Structural Materials of Guangdong Province, Shantou University, Shantou, Guangdong 515063, PR China

[⊥]Dalian Institute of Chemical Physics, Chinese Academy of Sciences, Dalian 116023, PR China

Supporting Information

ABSTRACT: This work demonstrates a novel photovoltaic application in which graphdiyne (GD) can be employed as a host material in a perovskite active layer for the first time. In the device fabrication, the best molar ratio for active materials is verified as $\text{PbI}_2/\text{MAI}/\text{GD}$ being 1:1:0.25, yielding a peak power-conversion efficiency of 21.01%. We find that graphdiyne, as the host material, exerts significant influence on the crystallization, film morphology, and a series of optoelectronic properties of the perovskite active layer. A uniform MAPbI_3 film with highly crystalline qualities, large domain sizes, and few grain boundaries was realized with the introduction of graphdiyne. Moreover, the current–voltage hysteresis was negligible, and device stability was significantly improved as well. The results indicate that graphdiyne as the host active material presents great potential for the enhancement of the performance of perovskite solar cells.

KEYWORDS: Graphdiyne, host active material, MAPbI_3 , perovskite device, solar cells



MAPbI_3 has been widely used as an active layer for solar cells since the organic hole-transport material of spiro-OMeTAD was applied to take the place of liquid electrolytes, leading to the significant improvement of stability and power conversion efficiency (PCE).¹ Carbon materials such as carbon nanotubes (CNTs), graphite, and graphene have attracted enormous attentions in the past decade and presented a large potential for perovskite solar cells (PSCs) owing to their remarkable electronic properties.^{2–4} All such materials have been reported to optimize the interface in PSCs in the literature. For example, CNTs can be employed as electrodes in PSCs, resulting in the impressive improvement of durability and stability compared with conventionally fabricated PSCs.² The modification of SnO_2 with graphene can enhance surface hydrophobicity and form van der Waals interaction between the surfactant and perovskite compounds, which significantly improves the performance of PSCs.³ A fullerene derivative (α -bis-PCBM) is applied as a templating agent for the solution processing of metal halide perovskite films, which tremendously boosts the performance and stability of PSCs.⁴ However, as we know, the dispersion of traditional carbon materials such as nanotube, graphite, and graphene still remains a challenge without sacrificing the favorable electronic

property. Meanwhile, the characteristics of zero band gap constrain their application in the field of photovoltaic devices.⁵

Graphdiyne (GD), a novel carbon material, possesses unique butadiyne linkages ($-\text{C}\equiv\text{C}-\text{C}\equiv\text{C}-$) in its highly π -conjugated structure, including benzene rings bonding with diacetylenic linkages.^{6,7} Such uniqueness endows GD with fascinating properties such as excellent electrical conductivity, favorable semiconducting properties, and superior chemical stability.^{8,9} What is more, GD is the first 2D carbon material that possesses a band gap as well as good solubility with dispersion in various solvent systems such as chlorobenzene, methanol, dimethylformamide, dimethyl sulfoxide, etc.^{10–12} Thus, the prospect of GD in photovoltaic devices is worth exploring. Most current researches related with GD focus on the optimization of interface layer in solar cells. In our previous works, GD is employed as a dopant into P3CT-K for improved hole-transporting property and doped in both PCBM and ZnO working as electron transport layers (ETLs),^{12,13} indicating that GD plays an essential role in the enhancement of both hole- and electron-transport efficiency. However, the topic of

Received: July 13, 2018

Revised: October 11, 2018

Published: October 22, 2018

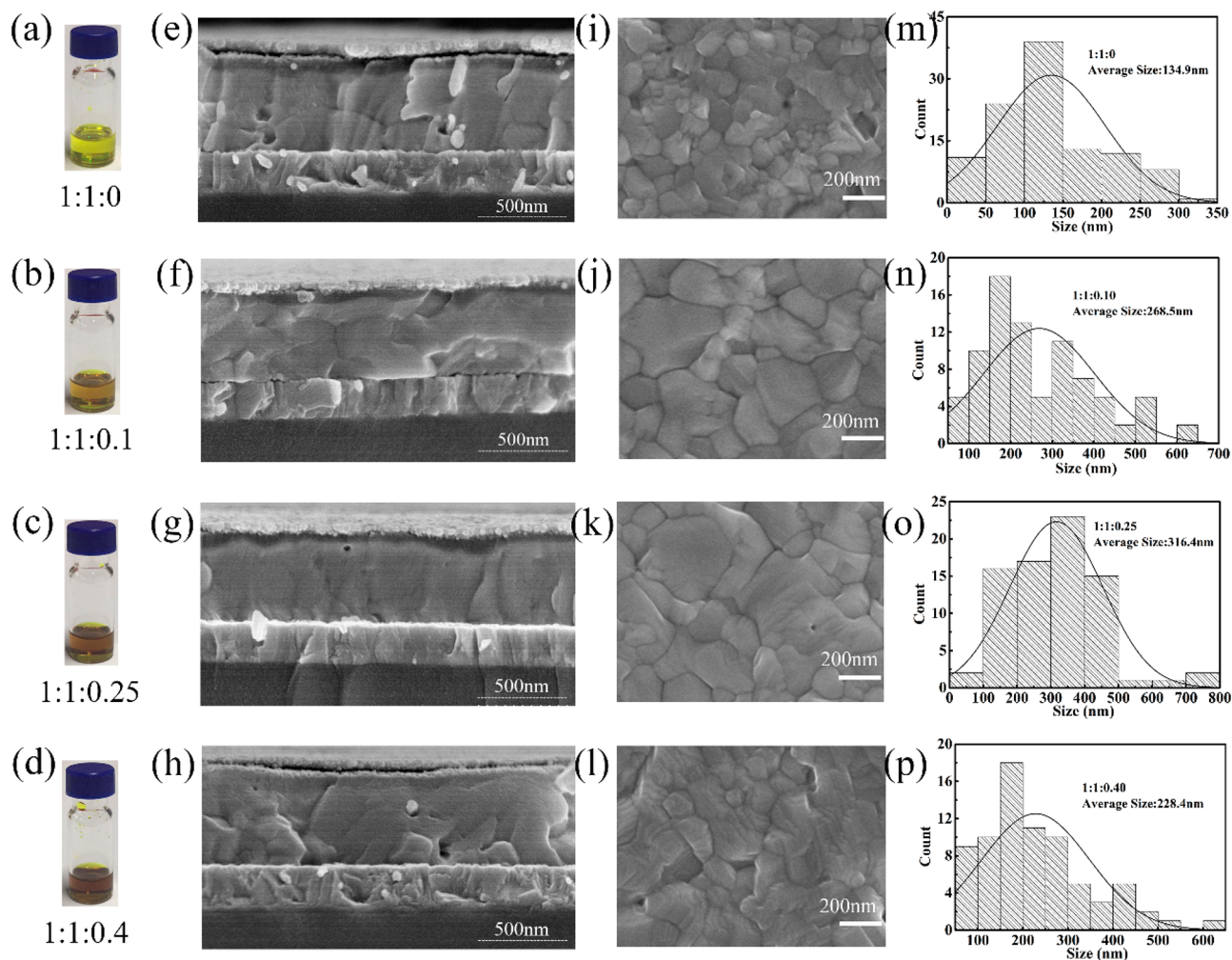


Figure 1. Photographs of the perovskite active layer with various molar ratios of GD: (a) 1:1:0, (b) 1:1:0.10, (c) 1:1:0.25, and (d) 1:1:0.40. (e–h) Cross-sectional SEM images and (i–l) planar SEM images of the perovskite active layer with various ratios of GD. (m–p) The distribution of the grain size of perovskite active layer with various ratios of GD.

the active semiconductor characteristics such as band gap and good solubility-based processing property is seldom devoted in the existing studies. This concern brings us to explore the possibility of applying GD into the active layer of perovskite solar cells.

In this paper, for the first time, we develop a simple approach to employ GD as a host material in the perovskite active layer. The best molar ratio of the active layer is $\text{PbI}_2/\text{MAI}/\text{GD} = 1:1:0.25$. We find that graphdiyne as the host material can improve the crystallization, film morphology, and a series of optoelectronic properties of the perovskite active layer. A uniform MAPbI_3 film with highly crystalline properties, large domain sizes, and few grain boundaries can be realized, which leads to a high efficiency of 21.01%. Simultaneously, GD can improve the transport efficiency of electrons and holes due to its bipolar nature of charge transport in the active layer. Our work demonstrates that graphdiyne as a host material is a promising strategy by which to enhance the performance of perovskite solar cells.

Figure 1a–d depicts the perovskite active layer with various GD ratios of (a) 1:1:0, (b) 1:1:0.10, (c) 1:1:0.25, and (d) 1:1:0.40. We can observe that the color of pure perovskite precursor is bright yellow, with the successive addition of corresponding molar weight of GD, the color of perovskite

precursor gets darker. Figure S1 shows the high-resolution TEM (HRTEM) characterization of GD, revealing that the layer-to-layer distance of GD was 0.350 nm. Figure S2 illustrates the Raman spectrum of GD, which presents characteristic peaks of 1377.9, 1595.9, and 2192.8 cm^{-1} . Considering the crucial role of morphology of perovskite layer and interlayer on achieving high performance of PSCs,^{14–16} the corresponding cross-sectional SEM were performed, and the results are displayed in Figure 1e–h. As shown, the pristine perovskite sample contains some pinholes, and the shape of crystals is irregular, which indicates that the growth of crystals is uneven. When the molar ratio is added to the 1:1:0.10 sample, the pinholes existing on cross-sectional perovskite decrease. With the molar ratio is added to 1:1:0.25, the pinholes disappear, and the crystals become more smooth and perpendicular to the substrate. Interestingly, when the molar ratio is added to the 1:1:0.40 sample, the pinholes show up and the shape of crystals becomes irregular again. To further confirm the role of GD as a host active material in perovskite active layer, planar SEM measurements of perovskite active layer with various ratios of GD were performed, as exhibited in Figure 1i–l. There are some pinholes at the top of the pristine perovskite sample, and the grain size is relatively small, with the mean size of 134.9 nm as is displayed in Figure 1m. With

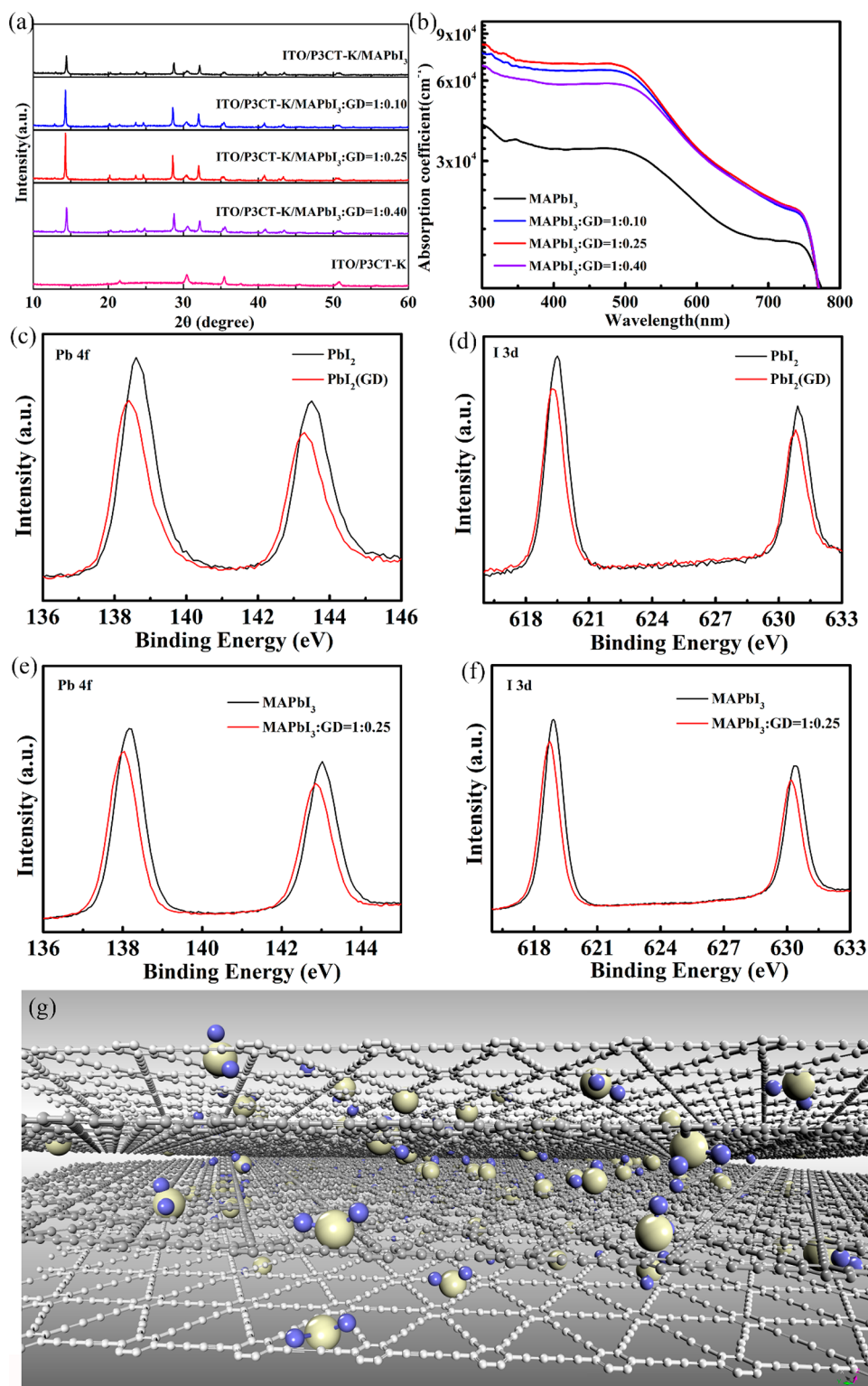


Figure 2. (a) X-ray diffraction patterns and (b) UV-vis absorption spectra of perovskite active layer with different molar ratios of GD. (c) XPS spectra of Pb 4f and (d) I 3d in PbI_2 and $\text{PbI}_2(\text{GD})$. (e) XPS spectra of Pb 4f and (f) I 3d in perovskite with different molar ratios of GD. (g) Schematic illustration of the adduct between GD and PbI_2 .

the molar ratio of 1:1:0.10, we can observe that the pinholes disappear, the grain size is increased to 268.5 nm in Figure 1n, and the roughness of the perovskite layer becomes smoother. When the molar ratio is added to the 1:1:0.25 sample, there are no pinholes existing on the film with the grain size further enlarged, as illustrated in Figure 1o, whose average size is

increased to 316.4 nm. Consequently, a uniform $\text{MAPbI}_3(\text{GD})$ film with large domain sizes and few grain boundaries is obtained. However, when the molar ratio is added to the 1:1:0.40 sample, the pinholes appear and the grain size is decreased to 228.4 nm, as displayed in Figure 1p. The surface of perovskite active layer becomes non-uniform. The measure-

ments of SEM suggest that GD as a host active material can greatly affect the grain size of the perovskite film, decrease the grain boundaries at an optimized ratio, and facilitate the formation of a uniform MAPbI₃(GD) film.

To further examine the crystallinity property, we conducted thin-layer X-ray diffraction (XRD) measurements for perovskite films deposited on ITO/P3CT-K substrates, as presented in Figure 2a. The crystal of perovskite displays diffraction peaks at 14.2°, 20.2°, 23.6°, 24.6°, 28.5°, 32.0°, 40.5°, and 43.3°, in accord with the reflections at (110), (112), (211), (202), (220), (310), (224), and (314), respectively, suggesting that the perovskite active layers have been completely transformed into a tetragonal phase.^{17,18} This can be found in the clearly increasing peak intensity of the crystal planes of the MAPbI₃ at 14.2° and 28.5° after the introduction of GD, which indicates enhanced crystallinity in the MAPbI₃ (GD) sample. What's more, at the very beginning, the crystallinity tends to be improved with the addition of GD. However, when the molar ratio of GD increases to 0.40, the crystallinity of perovskite is weakened, which implies that the overdose of GD has a negative impact on the crystallinity. The same explanation can be applied to different perovskite film morphologies with the variation of GD doses as well. As presented in Figure 2b, the MAPbI₃ perovskite films with GD exhibit a higher optical absorption coefficient compared to the pristine photoactive layer. The regularity is consistent with XRD results. The increased absorption coefficient of perovskite is conducive to a higher current density when the film is employed in the fabrication of PSCs.^{19,20}

To search for the reason for crystallinity enhancement, we performed X-ray photoelectron spectroscopy (XPS) to study the interaction between GD and perovskite. First, the interaction between GD and PbI₂ is investigated. As displayed in Figure 2c, the Pb 4f peaks in PbI₂(GD) are located at 138.4 and 143.3 eV, respectively, both of which are a ~0.2 eV shift to lower binding energy compared with those in PbI₂ (138.6 and 143.5 eV). Similarly, Figure 2d shows that the I 3d peaks in PbI₂(GD) located at 619.2 and 630.7 eV demonstrate ~0.3 and 0.2 eV shift to lower binding energy compared with 619.5 and 630.9 eV in PbI₂, respectively. The shifting of Pb 4f and I 3d peaks indicates the existence of additional negative charge around the Pb and I atoms. It is deduced that more electrons are accepted by Pb atom via coordinate bonding with GD, allowing the formation of the C–Pb bond, which generates an increased electron cloud density, resulting in a low electron affinity.²¹

Next, to examine the interaction between MAPbI₃ and GD, XPS of MAPbI₃ and MAPbI₃/GD = 1:0.25 was performed with results displayed in Figure 2e,f. Compared with Pb 4f peaks in PbI₂ (138.6 and 143.6 eV), the peaks in MAPbI₃ located at 138.2 and 143.0 eV, respectively, are observed to have a ~0.4 and 0.6 eV shift to a lower binding energy. Similarly, it is apparent that the shift of ~0.6 and ~0.5 eV to a lower binding energy appears when we compare the I 3d peaks in MAPbI₃ (618.9 and 630.4 eV) and PbI₂ (619.5 and 630.9 eV), respectively. As is known, PbI₂ falls into the category of hexagonal 2H polytype crystals and MAPbI₃ tetragonal crystals.^{17,21} When PbI₂ converts to MAPbI₃, I atoms surrounding Pb atoms are increased. Meanwhile, the negative charge around the Pb and I atoms increases due to the formation of tetragonal MAPbI₃ perovskite, which accounts for the shift of Pb 4f and I 3d peaks to lower binding energy. Comparatively, the Pb 4f peaks are found to exhibit a ~0.2 eV

shift to lower binding energy in MAPbI₃/GD (138.0 and 142.8 eV) in contrast to MAPbI₃ (138.2 and 143.0 eV), respectively. At the same time, Figure 2f shows the shift of I 3d peaks (a ~0.2 eV shift to lower binding energy) in MAPbI₃/GD located at 618.7 and 630.2 eV, compared with those in MAPbI₃ originating at 618.9 and 630.4 eV. It is known that iodide vacancies are easily formed during heat treatment due to the poor crystallinity of perovskite.²² The intermediate adduct of GD-PbI₂ can lead to a lower level of iodide vacancies in the crystal lattice, which results in the addition of I atoms surrounding Pb and I atoms in crystal, which is advantageous to the improvement of crystal quality and the stability of MAPbI₃.

Based on the above measurements of SEM, XRD, and XPS, we proposed a mechanism to expound the role of GD on the improved morphology and crystal quality of active layer. The intermediate adduct between GD and PbI₂ is formed after the addition of GD, as shown in Figure 2g, which can suppress the nucleation density thus increasing the growth space of crystal growth. Furthermore, with the formation of intermediate adduct, the critical free energy of nuclei is decreased with retarding the crystal growth of perovskite, which allows the crystal growing in the thermodynamically favorable inclination.²³ Moreover, the intermediate adduct of GD-PbI₂ can restrain the formation of iodide vacancies, which is beneficial for the improvement of crystal quality and the stability of MAPbI₃. All of the results are in good agreement and attest to the improvement of morphology and crystal quality of the active layer ascribed to the introduction of GD.

The GD in active layer serving as the host material is incorporated into PSCs devices with an architecture consisting of ITO/P3CT-K/MAPbI₃(GD)/PCBM/ZnO/Al, as depicted in Figure S3a. The detailed parameters are summarized in Table 1. As shown, the power conversion efficiency (PCE) of

Table 1. Summary of the Details of Devices Fabricated with Different Concentrations of GD in the Perovskite^a

active layer	V_{oc} (V)	J_{sc} (mA/cm ²)	FF (%)	PCE (%)	
				best	average
MAPbI ₃	1.047	21.2	75.1	16.69	16.28 (0.30)
MAPbI ₃ /GD, 1:0.10	1.066	23.3	79.2	19.64	19.19 (0.39)
MAPbI ₃ /GD, 1:0.25	1.073	24.3	80.1	21.01	20.46 (0.31)
MAPbI ₃ /GD, 1:0.40	1.039	22.8	78.7	18.68	18.29 (0.32)

^aAverage of 15 devices.

MAPbI₃(GD)-based devices is increased from 16.69% to 21.01% compared with those based on MAPbI₃ film without GD. In addition, to exclude the experiment accidental errors, the statistical data of 15 devices fabricated with different molar ratios of GD in MAPbI₃ are presented in a standard box plot in Figure S3b. It is observed that the values of J_{sc} , FF, and PCE of the devices with MAPbI₃ (GD) are enhanced remarkably. The results indicate that the devices with GD as the host material in perovskite solar cells can provide excellent reproducibility and favorable performance.

To figure out the effect of GD on the PSCs, current–voltage (J – V) curves are exhibited in Figure 3a. The device with GD as the host active material exhibits a peak PCE of 21.01% (average PCE of 20.46%), an open-circuit voltage (V_{oc}) of

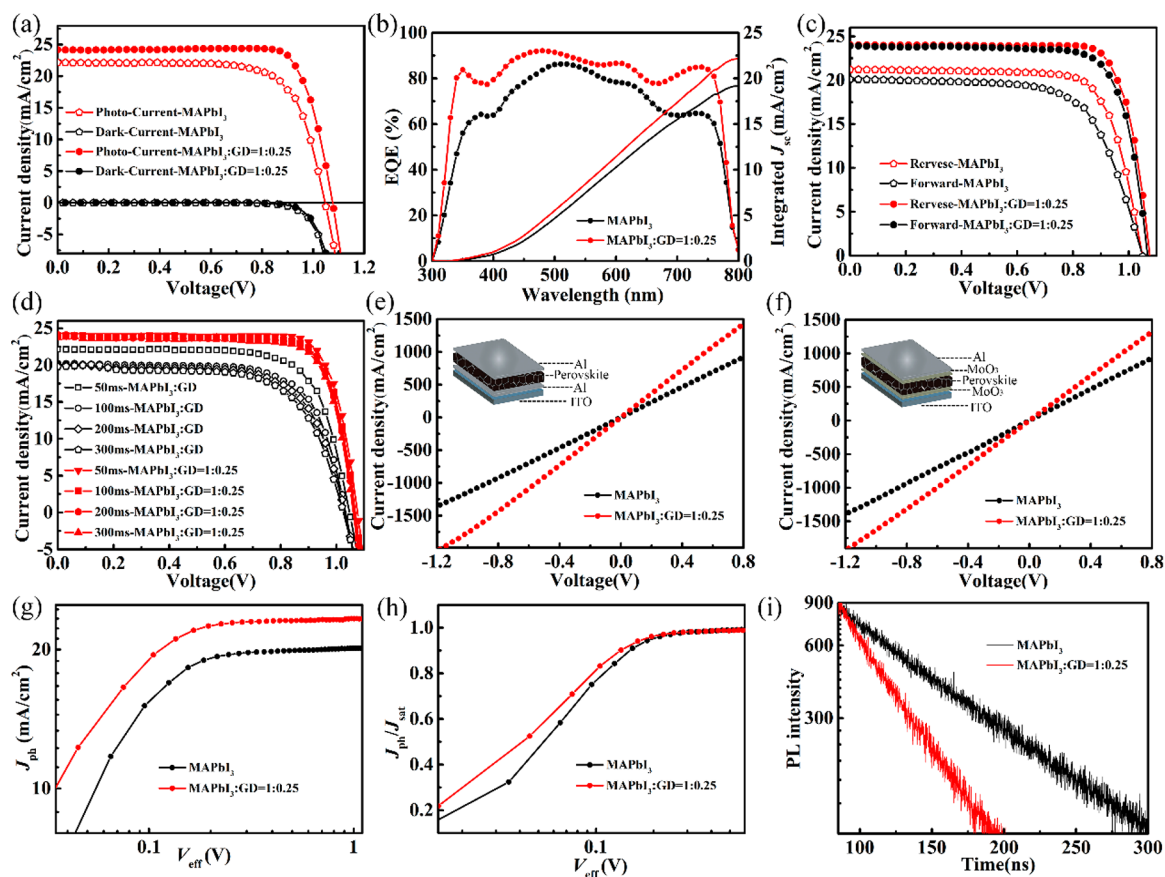


Figure 3. (a) Photocurrents and dark currents of the devices with or without GD. (b) Corresponding external quantum efficiency (EQE) spectra. (c) Data obtained from forward bias to short circuit (FB-SC) and from short circuit to forward bias (SC-FB) of the devices with or without GD. (d) Data obtained at the forward scan direction and different scanning rates with delay times of 50, 100, 200, or 300 ms. (e) J - V curves of electron-only devices with perovskite or perovskite (GD) active layers. The device structure is ITO/Al/perovskite or perovskite (GD)/Al. (f) J - V curves of hole-only devices with perovskite or perovskite (GD) active layers. The device structure is ITO/MoO₃/perovskite or perovskite (GD)/MoO₃/Al. (g) Plots of photocurrent density (J_{ph}) with respect to the effective bias (V_{eff}) in the devices with perovskite and perovskite (GD) as the ETLs. (h) Corresponding plots of J_{ph}/J_{sat} with respect to the effective bias (V_{eff}) in both devices. (i) The time-resolved PL of P3CT-K/perovskite/PCBM and P3CT-K/perovskite(GD)/PCBM on ITO substrates.

1.073 V, a short-circuit current (J_{sc}) of 24.3 mA cm⁻², and a fill factor (FF) of 80.1%, while MAPbI₃-based devices show a highest PCE of 16.69% (average PCE of 16.28%), a V_{oc} of 1.047 V, a J_{sc} of 21.2 mA cm⁻², and an FF of 75.1%. Corresponding external quantum efficiency (EQE) spectra of both devices are displayed in Figure 3b. It is observed that the EQE spectrum of the device with GD is obviously increased from the wavelength range of 300–800 nm compared to a MAPbI₃-based device, which is in agreement with the J_{sc} obtained from the J - V results shown above. The J - V curves of the devices based on MAPbI₃ or MAPbI₃(GD) with different scanning directions were recorded, as shown in Figure 3c. The PCE values obtained from the forward bias scan (forward bias to short circuit, FB-to-SC) and the reverse-bias scan (short circuit to forward bias, SC-to-FB) of devices with GD are 21.0% and 19.7%, respectively, while the counterparts of the reference devices are 16.7% and 14.2%, respectively. The PCE values of the devices with GD exhibit a smaller disparity between forward bias scan and the reverse bias scan compared with the reference devices. It is proposed that the introduction of GD as the host material can decrease the charge accumulations, resulting in an easier charge-transfer passage-way and reduced charge accumulations.^{11,12} Therefore, the J - V hysteresis is improved significantly. In addition, the J - V

curves of MAPbI₃(GD)-based devices at different scanning rates with delay time ranging from 50, 100, 200, to 300 ms were also examined in Figure 3d. The J - V curves at different scanning rates are almost overlapping with each other. These results indicate that the photocurrent hysteresis could be mitigated to a certain extent by incorporating GD in active layers. The improved photocurrent hysteresis in MAPbI₃(GD)-based devices may be ascribed to the enhanced electrical properties. To understand the origin of the J_{sc} increment, the J - V curves of hole-only devices with the structure of ITO/Al/MAPbI₃ or MAPbI₃(GD)/Al and ITO/MoO₃/MAPbI₃ or MAPbI₃(GD)/MoO₃/Al were measured to test their hole-extraction behaviors.^{24,25} In Figure 3e,f, the J - V curves show that GD, as the host active layer, exhibits higher current density at the same forward bias than the undoped one, indicating a better capability of electron and hole extraction of MAPbI₃(GD). The G_{max} and P values are plotted in Figure 3g,h to investigate the influence of MAPbI₃(GD) on the PSCs.^{26,27} From Figure 3g, with the increase of effective voltage, the saturation photocurrent (J_{sat}) in the device with MAPbI₃(GD) reaches earlier than that with MAPbI₃. Generally, the saturated photocurrent correlates to the maximum exciton generation rate (G_{max}). The values of G_{max} for the MAPbI₃- and MAPbI₃(GD)-based devices are 4.74 ×

10^{26} and $5.50 \times 10^{26} \text{ m}^{-3} \text{ s}^{-1}$, respectively. An enhancement of G_{max} is found in the $\text{MAPbI}_3(\text{GD})$ -based devices. It is noted that the exciton dissociation probability (P) obtained from the normalized photocurrent density $J_{\text{ph}}/J_{\text{sat}}$ is appreciably different among three devices, as shown in Figure 3h. For example, at 0.1 V of V_{eff} the P value is 77% for the device based on MAPbI_3 and 82% for the device with $\text{MAPbI}_3(\text{GD})$ as the active layer, respectively. The increase of the P value implies the reduction of the exciton recombination rate. The results suggest that G_{max} is increased and the exciton recombination is suppressed when $\text{MAPbI}_3(\text{GD})$ served as the active layer, thus leading to better J_{sc} and FF values. The stabilized photocurrent output of the optimal $\text{MAPbI}_3(\text{GD})$ -based device was measured. The maximal steady-state power is set to 0.862 V, and the photocurrent output is illustrated in Figure S4. The results indicate that the optimized PCE in our device is reliable.^{28,29} The measurements of steady-state photoluminescence (PL) and time-resolved PL were performed for P3CT-K/perovskite/PCBM, and P3CT-K/perovskite(GD)/PCBM on ITO substrates to study the effect of GD. It is observed from Figure S5 that the steady-state PL of $\text{MAPbI}_3(\text{GD})$ film was quenched. Furthermore, we observed the blue shift of the PL peak for the $\text{MAPbI}_3(\text{GD})$ film-based substrate. Those indicate a reduced defects states of $\text{MAPbI}_3(\text{GD})$ film, which results in the enhanced FF and PCE of the device by decreasing the nonradiative recombination. As shown in Figure 3i, the average carrier lifetime of pure MAPbI_3 and $\text{MAPbI}_3(\text{GD})$ are 73.3 and 16.8 ns. The result indicates a faster transfer of charge for $\text{MAPbI}_3(\text{GD})$ film, which leads to increased J_{sc} and PCE values.^{13,26}

The stability measurements of the solar cells with or without GD as the host active material were further performed. All of the devices were stored and measured in the nitrogen-filled glovebox without any encapsulation. The stability measurements were recorded periodically. Performance data based on devices with different active layers are represented as a standard box plot in Figure 4. The devices with GD exhibit significantly improved stability compared with the reference ones. All of the parameters of V_{oc} , J_{sc} , FF, and PCE of the control ones are decreased remarkably. The PCE of $\text{MAPbI}_3(\text{GD})$ -based devices remains about 85% after the storage of 33 days, better than the pristine MAPbI_3 value of about 30% maintenance, which indicates that employing GD as the host active material is an effective way to improve the device stability. To figure out the reason of the stability improvement, we conducted thin-layer XRD measurements for perovskite films deposited on ITO/P3CT-K substrates after 30 days stored in the nitrogen-filled glovebox without any encapsulation. As shown in the Figure S6a,b, it is observed that the PbI_2 signals are weakened after the addition of GD, which contributes to the stability enhancement. We think that the enhanced crystallinity and lower degree of decomposition due to the addition of GD are responsible for the decrease of PbI_2 signals.³⁰ However, as exhibited in Figure S6c, the intermediate adduct of GD-PbI_2 can restrain the formation of iodide vacancies in crystal grow, which is beneficial for the improvement of crystal quality and the stability of MAPbI_3 , as proven by the XPS results.

In summary, graphdiyne was used as the host material in solar cells for the first time. It was also the first time that carbon materials were used in a perovskite active layer, yielding a peak PCE of 21.01%. The introduction of graphdiyne can improve the morphology and crystal quality of active layer,

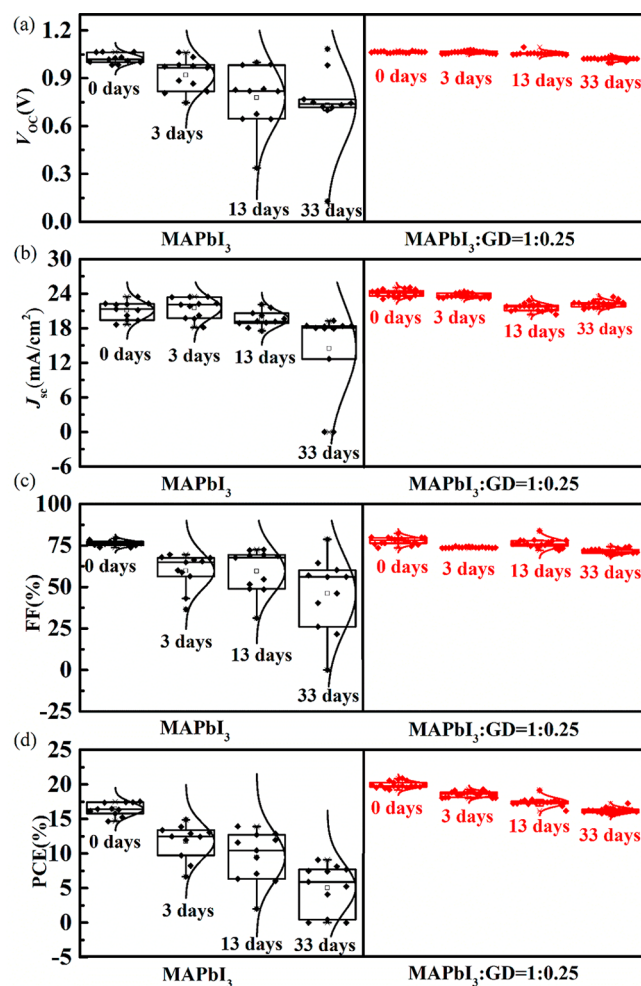


Figure 4. Stability tests of devices with different active layers are represented as a standard box plot shown in (a) V_{oc} , (b) J_{sc} , (c) FF, and (d) PCE. A total of 11 devices were used for perovskite-based PSCs, and 18 devices were used for perovskite (GD)-based PSCs.

leading to a uniform MAPbI_3 film with highly crystalline properties, large domain sizes, and few grain boundaries. From the intermediate adduct GD-PbI_2 , Pb atom accepts more electrons via coordinate bonding with GD, which restrains the formation of iodide vacancies and contributes to the improvement of crystal quality and the stability of MAPbI_3 , proved by the XPS results. Moreover, the J - V hysteresis is significantly improved as well. The results indicate that applying graphdiyne as the host active material is a promising strategy to improve the crystalline quality of the active layer and enhance the performance of perovskite solar cells.

Experimental Section. The details of material and characterizations, device fabrications, and measurements are provided in the Supporting Information.

■ ASSOCIATED CONTENT

Supporting Information

The Supporting Information is available free of charge on the ACS Publications website at DOI: 10.1021/acs.nanolett.8b02863.

Figures showing TEM analysis, a Raman spectrum, experimental schematic diagrams, performance data, steady-state efficiency and PL results, and XRD patterns; additional experimental details (PDF)

AUTHOR INFORMATION

Corresponding Authors

*E-mail: jiutg@qibebt.ac.cn.

*E-mail: ylli@iccas.ac.cn.

ORCID

Tonggang Jiu: 0000-0001-9608-4429

Fushen Lu: 0000-0002-3323-7181

Yuliang Li: 0000-0001-5279-0399

Author Contributions

Y.L. and T.J. contributed the idea. J.L. discussed the experimental plan and conducted the corresponding device fabrication and characterization. S.C. drew the schematic illustration. All of the authors contributed with regard to data analysis and the composition of the manuscript.

Notes

The authors declare no competing financial interest.

ACKNOWLEDGMENTS

The study was supported by the Major Program of Shandong Province Natural Science Foundation (grant no. ZR2017ZB0313). The project was supported by National Natural Science Foundation of China (grant no. 51672288) and Youth Innovation Promotion Association of Chinese Academy of Sciences. This study was also supported by DICP QIBEBT (grant no. UN201705), the Dalian National Laboratory For Clean Energy and Open Foundation of Key Laboratory for Preparation and Application of Ordered Structural Materials of Guangdong Province.

REFERENCES

- (1) Kim, H. S.; Lee, C. R.; Im, J. H.; Lee, K. B.; Moehl, T.; Marchioro, A.; Moon, S. J.; Humphry-Baker, R.; Yum, J. H.; Moser, J. E.; Grätzel, M.; Park, N. G. *Sci. Rep.* **2012**, *2*, 591.
- (2) Zhao, X.; Tao, L.; Li, H.; Huang, W.; Sun, P.; Liu, J.; Liu, S.; Sun, Q.; Cui, Z.; Sun, L.; Shen, Y.; Yang, Y.; Wang, M. *Nano Lett.* **2018**, *18*, 2442–2449.
- (3) Zheng, X.; Chen, H.; Li, Q.; Yang, Y.; Wei, Z.; Bai, Y.; Qiu, Y.; Zhou, D.; Wong, K. S.; Yang, S. *Nano Lett.* **2017**, *17*, 2496–2505.
- (4) Zhang, F.; Shi, W.; Luo, J.; Pellet, N.; Yi, C.; Li, X.; Zhao, X.; Dennis, T. J. S.; Li, X.; Wang, S.; Xiao, Y.; Zakeeruddin, S. M.; Bi, D.; Grätzel, M. *Adv. Mater.* **2017**, *29*, 1606806.
- (5) Nayebi, P.; Zaminpayma, E. *Phys. B* **2017**, *521*, 112–121.
- (6) Xue, Y.; Li, Y.; Zhang, J.; Liu, Z.; Zhao, Y. *Sci. China: Chem.* **2018**, *61*, 765.
- (7) Huang, C.; Li, Y. *Acta Phys. Chim. Sin.* **2016**, *32*, 1314–1329.
- (8) Li, Y. *Zhongguo Kexue: Huaxue* **2017**, *47*, 1045–1056.
- (9) Li, Y.; Xu, L.; Liu, H.; Li, H. *Chem. Soc. Rev.* **2014**, *43*, 2572–2586.
- (10) Chen, C.; Li, J.; Sheng, X.-L. *Phys. Lett. A* **2017**, *381*, 3337–3341.
- (11) Chen, Y.; Liu, H.; Li, Y. *Chin. Sci. Bull.* **2016**, *61*, 2901–2912.
- (12) Li, J.; Zhao, M.; Zhao, C.; Jian, H.; Wang, N.; Yao, L.; Huang, C.; Zhao, Y.; Jiu, T. *ACS Appl. Mater. Interfaces* **2018**, DOI: 10.1021/acsami.8b02611.
- (13) Li, J.; Jiu, T.; Duan, C.; Wang, Y.; Zhang, H.; Jian, H.; Zhao, Y.; Wang, N.; Huang, C.; Li, Y. *Nano Energy* **2018**, *46*, 331–337.
- (14) Lee, J. W.; Kim, S. G.; Bae, S. H.; Lee, D. K.; Lin, O.; Yang, Y.; Park, N. G. *Nano Lett.* **2017**, *17*, 4270–4276.
- (15) Zhao, Y.; Tan, H.; Yuan, H.; Yang, Z.; Fan, J. Z.; Kim, J.; Voznyy, O.; Gong, X.; Quan, L. N.; Tan, C. S.; Hofkens, J.; Yu, D.; Zhao, Q.; Sargent, E. H. *Nat. Commun.* **2018**, *9*, 1607.
- (16) Gong, X.; Sun, Q.; Liu, S.; Liao, P.; Shen, Y.; Grätzel, C.; Zakeeruddin, S. M.; Grätzel, M.; Wang, M. *Nano Lett.* **2018**, *18*, 3969–3977.

(17) Wang, Y.-C.; Li, X.; Zhu, L.; Liu, X.; Zhang, W.; Fang, J. *Adv. Energy Mater.* **2017**, *7*, 1701144.

(18) Liang, P. W.; Liao, C. Y.; Chueh, C. C.; Zuo, F.; Williams, S. T.; Xin, X. K.; Lin, J.; Jen, A. K. *Adv. Mater.* **2014**, *26*, 3748–3754.

(19) Im, J. H.; Jang, I. H.; Pellet, N.; Grätzel, M.; Park, N. G. *Nat. Nanotechnol.* **2014**, *9*, 927–932.

(20) Smith, I. C.; Hoke, E. T.; Solis-Ibarra, D.; McGehee, M. D.; Karunadasa, H. I. *Angew. Chem., Int. Ed.* **2014**, *53*, 11232–11235.

(21) Wang, Y.-C.; Chang, J.; Zhu, L.; Li, X.; Song, C.; Fang, J. *Adv. Funct. Mater.* **2018**, *28*, 1706317.

(22) Bi, D.; Yi, C.; Luo, J.; Décoppet, J.-D.; Zhang, F.; Zakeeruddin, S. M.; Li, X.; Hagfeldt, A.; Grätzel, M. *Nat. Energy* **2016**, *1*, 16142.

(23) Ummadisingu, A.; Steier, L.; Seo, J. Y.; Matsui, T.; Abate, A.; Tress, W.; Grätzel, M. *Nature* **2017**, *545*, 208–212.

(24) Chen, W.; Wu, Y.; Yue, Y.; Liu, J.; Zhang, W.; Yang, X.; Chen, H.; Bi, E.; Ashraful, I.; Grätzel, M.; Han, L. *Science* **2015**, *350*, 944–948.

(25) Chen, W.; Liu, F.; Feng, X.; Djurišić, A. B.; Chan, W.; He, Z. *Adv. Energy Mater.* **2017**, *7*, 1700722.

(26) Li, J.; Duan, C.; Wang, N.; Zhao, C.; Han, W.; Jiang, L.; Wang, J.; Zhao, Y.; Huang, C.; Jiu, T. *ACS Appl. Mater. Interfaces* **2018**, *10*, 17401–17408.

(27) Mihailetschi, V. D.; Xie, H. X.; de Boer, B.; Koster, L. J. A.; Blom, P. W. M. *Adv. Funct. Mater.* **2006**, *16*, 699–708.

(28) Kuang, C.; Tang, G.; Jiu, T.; Yang, H.; Liu, H.; Li, B.; Luo, W.; Li, X.; Zhang, W.; Lu, F.; Fang, J.; Li, Y. *Nano Lett.* **2015**, *15*, 2756–2762.

(29) Lee, J. W.; Kim, S. G.; Bae, S. H.; Lee, D. K.; Lin, O.; Yang, Y.; Park, N. G. *Nano Lett.* **2017**, *17*, 4270–4276.

(30) Li, X.; Yi, C.; Ibrahim Dar, M.; Tschumi, L. M.; Zakeeruddin, S. M.; Han, M. K.; Nazeeruddin, H.; Grätzel, M.; Luo, J. *Nat. Chem.* **2015**, *7*, 703–711.